Electronic Supplementary Material (ESI) for Journal of Materials Chemistry A
This journal is © The Royal Society of Chemistry 2013

Effect of iron-carbide formation on the number of active sites in Fe-N-C catalysts for the oxygen reduction reaction (ORR) in acidic media

Ulrike I. Kramm,[a,b]*, Iris Herrmann-Geppert,[ac] Sebastian Fiechter,[a] Gerald Zehl,[a] Ivo Zizak,[d] Iris Dorbandt,[a] Dieter Schmeißer,[b] and Peter Bogdanoff[a]

[a] Helmholtz-Center Berlin for Materials and Energy, Institute of Solar Fuels, Hahn-Meitner-Platz 1, 14109 Berlin, Germany

[b] Brandenburgische Technische Universität Cottbus-Senftenberg, Chair of Applied Physics and Sensors, Konrad-Wachsmann-Allee 17, 03046 Cottbus, Germany, * E-Mail: kramm@tu-cottbus.de, Tel. +49-355+69-2972

[c] Helmut-Schmidt-University, Functional Materials, Holstenhofweg 85, 22043 Hamburg, Germany and

Helmholtz Centre Geesthacht, Institute for Materials Research, Max-Planck-Str. 1, 21502 Geesthacht, Germany

[d] Helmholtz-Center Berlin for Materials and Energy, BESSY II, Albert-Einstein-Str. 15, 12489 Berlin, Germany

Supplementary Information

1. Analysis of the heat-treatment process of the FeTMPPCl+iron-oxalate-dihydrate precursors with or without sulfur by TG-MS and HT-XRD.

2. Physical characterization of H_2/Fe-S and H_2/Fe+S catalysts by XRD, Mößbauer and Raman spectroscopy

3. Summary of the Mößbauer parameters, relative absorption areas and assignment to iron species

4. TEM images of the Fe/Fe-S catalyst

5. RDE curves (rpm 200, 400, 900) of all standard catalysts (Fe/Fe-S, Fe/Fe+S, H_2/Fe-S, H_2/Fe+S)

6. Comparison of the effect of a second heat-treatments in N_2 and NH_3 on the kinetic current density for the reference catalyst (Fe/KB600) and the Fe/Fe+S catalyst.

1. Analysis of the heat-treatment process of the FeTMPPCl+iron-oxalate-dihydrate precursors with or without sulfur by TG-MS and HT-XRD.

In Figure S1 the thermogravimetric measurements (top graphs) together with the temperature-dependent mass fragments of the released gaseous reaction products (bottom graphs) are shown. The solid reaction products dominating the X-ray diffractograms obtained by HT-XRD are given in Figure S2 for selected temperatures, representative for the heat-treatment process.

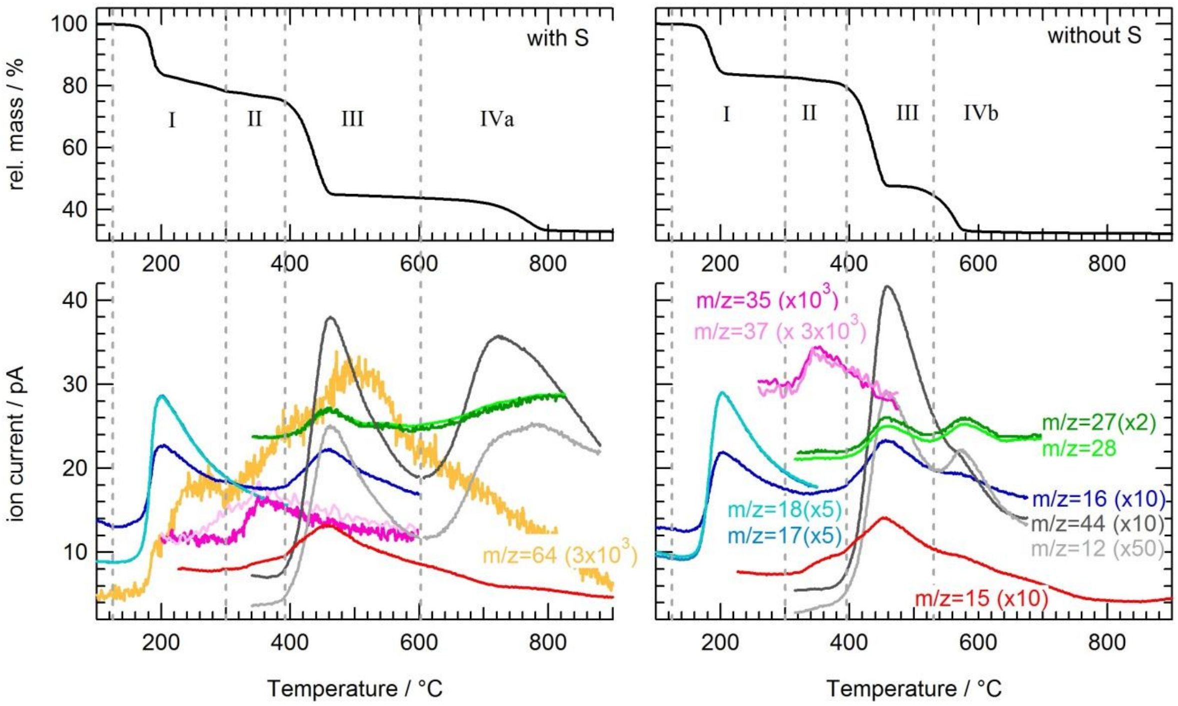

Fig. S1. Thermogravimetry for the sulfur-containing (left) and sulfur-free (right) precursor mixtures. The samples were heated with 7.5 °C/min in He atmosphere. Top graphs show the change of mass during the heating process and the bottom graphs the related mass fragments. For better visualization some compounds were enlarged with the factors as indicated, factors were always chosen similar for both precursor samples.

Table S1. Assignment of the different gaseous decomposition products to the detected mass fragments.

Decomposition product	Origin	Detected Ions / Mass fragments
CO_2	Iron oxalate dihydrate	CO_2^+ (m/z = 44), CO^+ (m/z = 28), O^+ (m/z = 16), C^+ (m/z = 12)
H_2O	Iron oxalate dihydrate	H_2O^+ (m/z = 18), OH^+ (m/z = 17), O^+ (m/z = 16)
Methoxyphenyl	FeTMPPCl	CH_3^+ (m/z = 15)
Chlorine	FeTMPPCl	Cl^+ (m/z = 35, m/z = 37)
FeN_4	FeTMPPCl	HCN^+ (m/z = 27), N_2^+ (m/z = 28), NH^+ (m/z = 15)
Sulfur	Sulfur	S_2^+ or SO_2^+ (m/z = 64)

A first observation of both Figures allows the conclusion that up to 500°C the heat-treatment process remains basically the same. One exception is related to the release of sulfur-containing compounds over nearly the complete investigated temperature range for the precursor mixture prepared under the addition of sulfur. Both precursors reveal three main decomposition steps (I, II, IV) and a fourth (II) that can only be identified by the mass fragments.

The first decomposition step I (starting at ~ 150 °C) is related to the release of crystal water from the iron-oxalate dihydrate as identified by the corresponding mass signals and the change of the XRD patterns. The reaction is given in equation 1.

T = 150°C: $FeC_2O_4 \cdot 2\ H_2O \rightarrow FeC_2O_4 + 2\ H_2O \uparrow$ (eq. 1)

Afterwards chlorine is detected by the mass spectrometer (range II) indicating the change of the fivefold coordination of the FeTMPPCl to a fourfold coordinated FeTMPP. From previous investigation of the temperature-dependent changes observed for carbon-supported FeTMPPCl it is known that at 400°C less than 10% of the initially present Cl-$Fe^{3+}N_4$-centers are still present.[1] Due to the low mass-ratio of chlorine in the overall precursor mixture (< 1%); however, no significant change of the relative mass can be found. During the main reaction step between 400 – 450 °C (range III) iron oxalate decomposes under the release of carbon di- and monoxide to iron oxide ($Fe_{1-x}O$) (Eq. 2).

T = 400-450°C: $FeC_2O_4 \cdot xH_2O \rightarrow FeO + CO_2 \uparrow + CO \uparrow + H_2O \uparrow$ (eq. 2)

Besides CO and CO_2, also the release of methoxyphenyl can be detected (m/q = 15), indicating the beginning of carbonization of the porphyrin molecule.[2] This carbonization step is accompanied by a partial decomposition of FeN_4-centers (m/q = 27, 28). Please note: for the carbon-supported FeTMPPCl no decomposition of FeN_4-centers was found up to 600°C.[3]

T = 400-450°C: $FeTMPP \rightarrow FeN_4 + C_6H_5 \uparrow + CH_3 \uparrow$ (eq. 3)

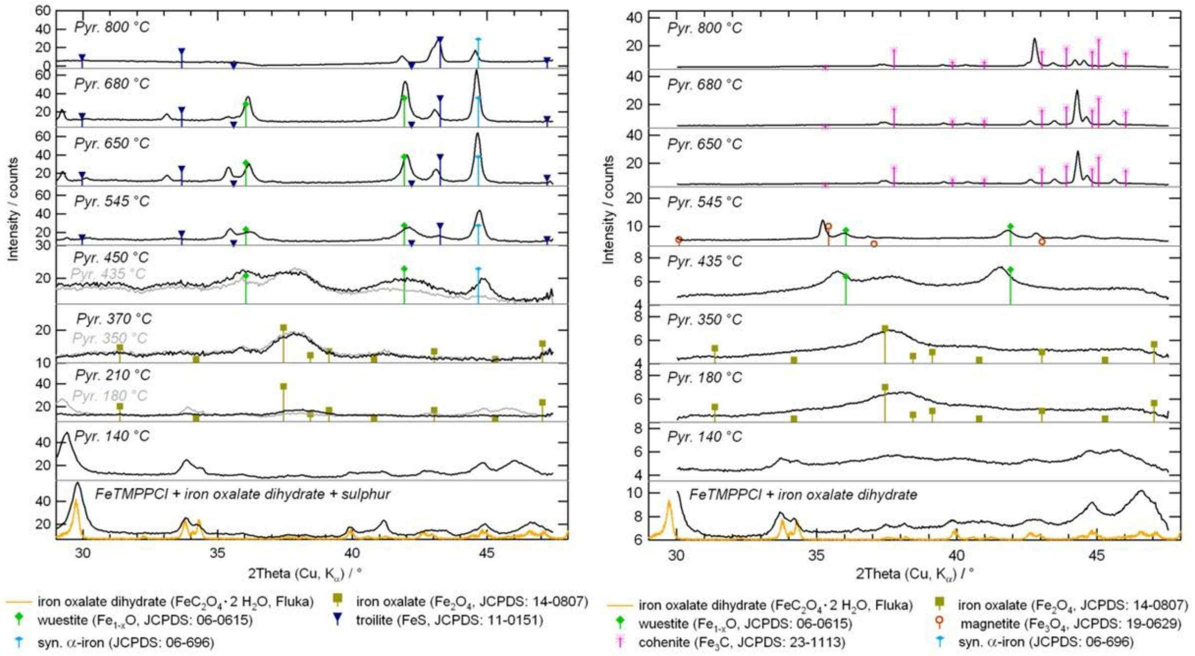

Fig. S2: X-ray diffractograms extracted from in-situ HT-XRD measurements.

The third decomposition step of the sulfur-free precursor is found for T = 520 °C (range IVb). The release of carbon dioxide indicates that this decomposition step is attributed to the reduction of the previously formed iron oxide (FeO, eq. 2) to elemental iron and iron carbide by the already formed carbon (eq. 4). This interpretation is supported by the high-temperature diffractograms. In the same temperature range, again HCN and N_2 are detected indicating a second decomposition of FeN_4-centers.

T = 520 – 650°C: $3\ FeO + C \rightarrow Fe_3C + 3/2\ O_2 \uparrow$ (eq. 4)

Comparing these results to those obtained for the sulfur-containing precursor, it is observed that this third decomposition step is shifted to higher temperatures (range IVa, starting at about 650/700°C). Basically CO_2-fragments are found. From HT-XRD data; however, no formation of iron carbide is found. In contrast only troilite and alpha-iron are detected as crystalline phases in the 800°C diffractogram. It can be concluded that during the reduction step (eq.4) iron or iron carbide reacts immediately with the present sulfur under the formation of iron sulfide. Furthermore, it is important to note, that in contrast to the sulfur-free precursor, there is no second FeN_4-decomposition peak.

2. Physical characterization of H_2/Fe-S and H_2/Fe+S catalysts by XRD, Mößbauer and Raman spectroscopy

In Figure S3 the physical characterization of the H_2/Fe-S and H_2/Fe+S catalysts are given (i.e. after heat-treatment to 800°C and subsequent acid-leaching). The H_2TMPP-based catalysts reveal the same trends as observed for the FeTMPPCl-related compounds:

- Only the sulfur-free catalyst shows reflexes within the diffractogram that can be assigned to graphite and cohenite, which is in accordance with the HT-XRD data.

- From the Raman data it can be concluded that the graphene-layer extension is smaller and the state of graphitization is higher for H_2/Fe-S compared to H_2/Fe+S.

- The Mößbauer spectrum of the H_2/Fe+ S catalyst contains only different FeN_4-centers and small quantities of super-paramagnetic iron, whereas the H_2/Fe-S catalyst shows strong absorption lines assigned to iron carbide but only a small absorption intensity related to FeN_4-centers.

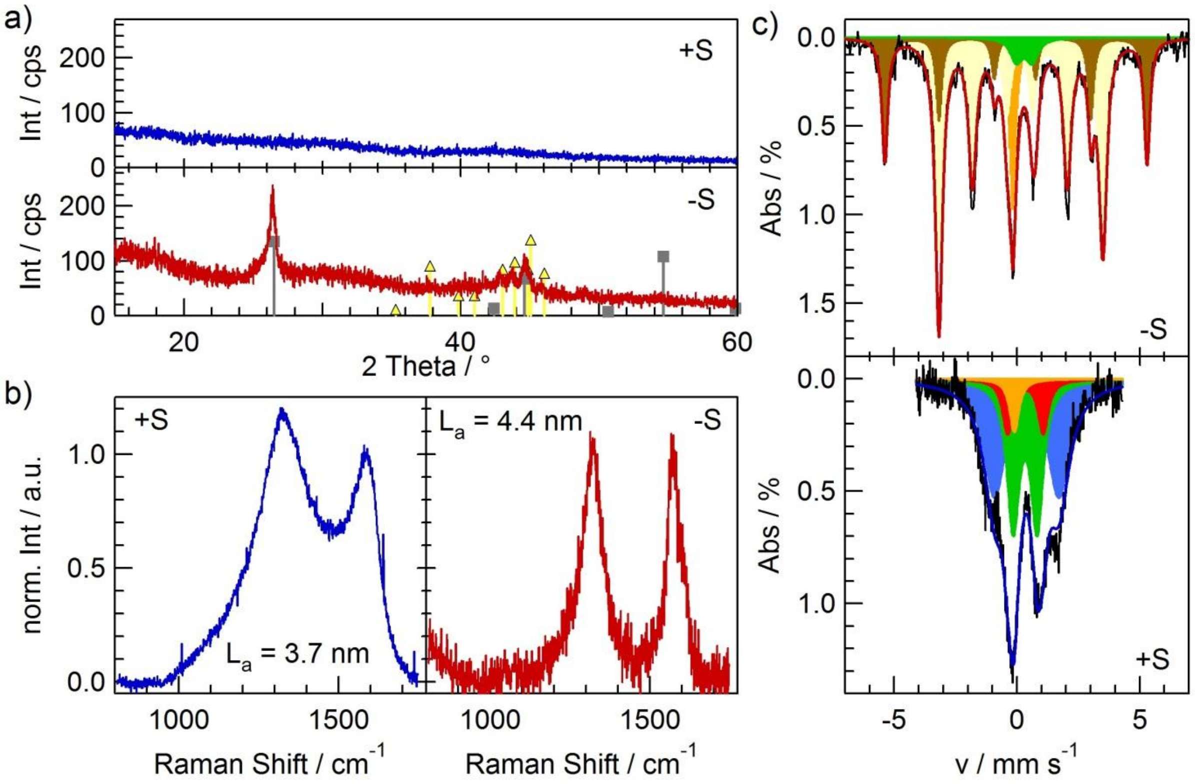

Fig. S3. Physical characterization of the H_2/Fe+S (–) and H_2/Fe-S (–) catalysts by X-ray diffraction (a), Raman spectroscopy (b) and Mößbauer spectroscopy (c). The diffraction patterns are assigned to cohenite (Δ) and graphite (□).

3. Summary of the Mößbauer parameters, relative absorption areas and assignment to iron species

Table S2. Summary of the Mößbauer parameters, relative absorption areas and assignment to iron species for all catalysts studied in this work. If an iron species is present in more than one catalyst, the values of the Mößbauer parameters denote the average of all.

	δ_{Iso}	ΔE_Q	fwhm	H_0 / T	Fe/Fe-S	Fe/Fe+S	H_2/Fe-S	H_2/Fe+S	Assignment
	/ mm s^{-1}				Area / %				
Sing	-0.14 (0.03)	-	0.33 (0.07)	-	0	2.7 (1.9)	10.0 (0.5)	5.0 (0.2)	superparamagnetic iron [4]
D1	0.29 (0.02)	0.81 (0.16)	0.66 (0.16)	-	10.7 (1.4)	58.5 (4.2)	5.1 (0.6)	60.4 (1.1)	FeN$_4$ (2+, low-spin) [3,5,6]
D2	0.27 (0.01)	2.99 (0.01)	0.90 (0.05)	-		21.9 (4.4)		23.0 (0.6)	FeN$_4$ (2+, midd-spin), like FePc [7,8]
D3	0.36 (0.03)	1.87 (0.12)	0.68 (0.08)	-		16.9 (4.7)		11.6 (1.3)	FeN$_4$ (like [FePc]$^{2-}$) [8]
Sext1	0.16 (0.02)	0.02 (0.01)	0.36 (0.02)	20.7 (0.1)	78.5 (6.9)		59.5 (0.8)		iron carbide [4]
Sext2	0.08 (0.03)	-0.09 (0.03)	0.21 (0.04)	20.2 (0.2)	10.8 (5.1)				iron carbide [4]
Sext3	-0.06 (0.01)	0.04 (0.01)	0.28 (0.01)	33.2 (< 0.1)			25.4 (0.7)		alpha iron / iron carbide [4]

4. TEM images of the Fe/Fe-S catalyst

The TEM images indicate that the iron / iron-carbide particles present in the Fe/Fe-S catalysts are surrounded by a few layers of graphene.

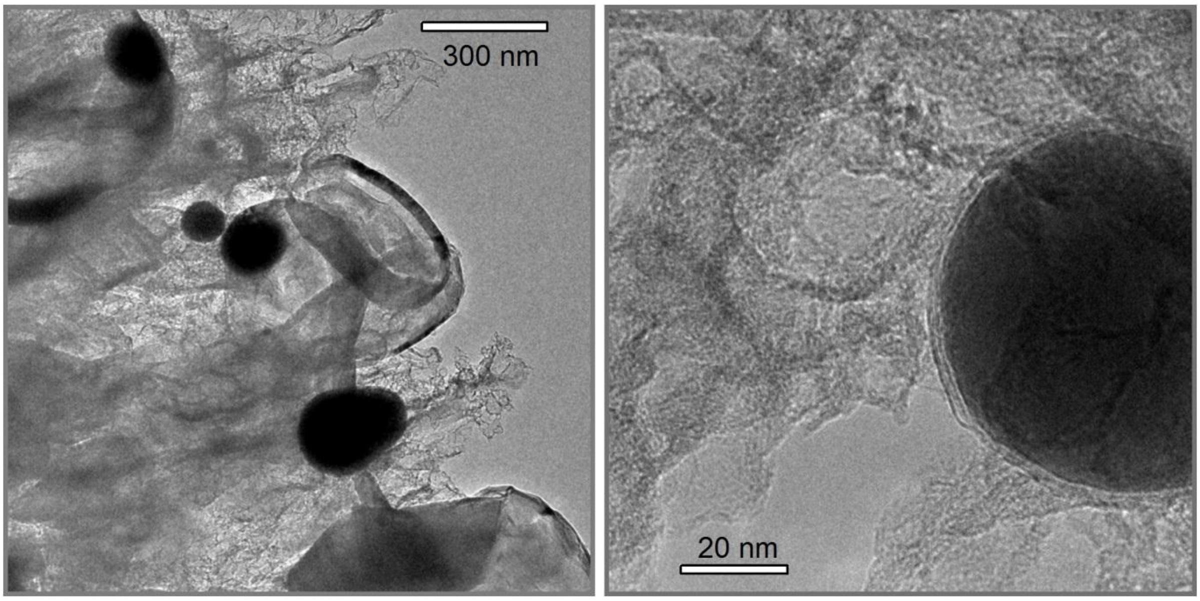

Fig. S4. TEM images of the Fe/Fe-S catalyst.

5. RDE curves of all standard catalysts (Fe/Fe-S, Fe/Fe+S, H_2/Fe-S, H_2/Fe+S)

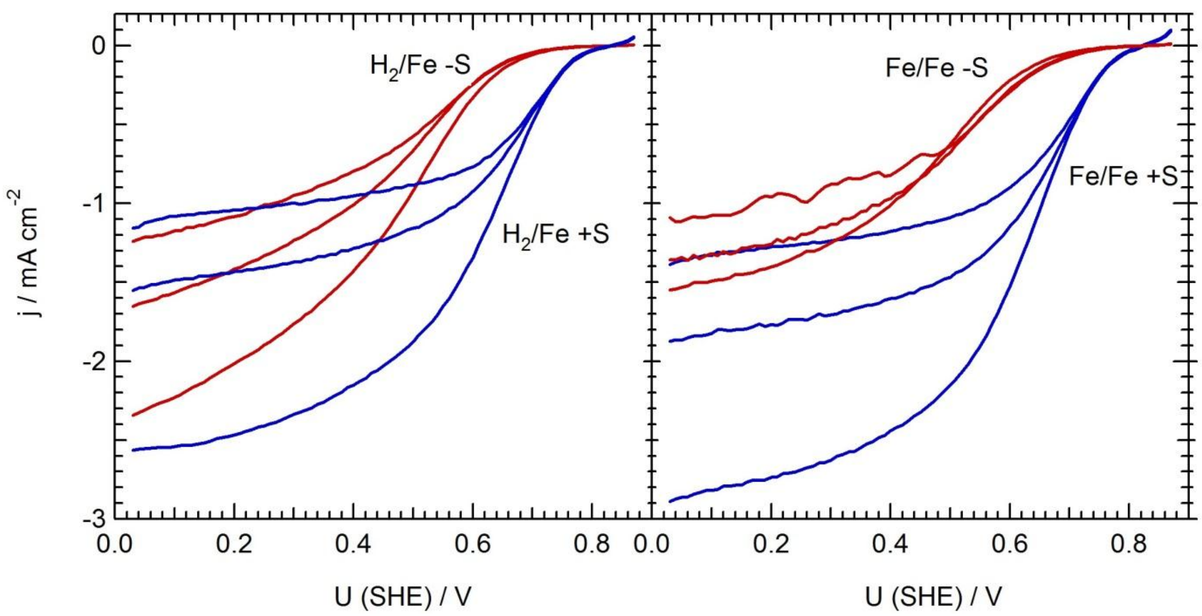

Fig. S5. RDE measurements (at rpm 200, 400 and 900) of the different standard catalysts studied in this work (measurements were performed in 0.5M H_2SO_4).

6. Comparison of the effect of second heat-treatments in either N_2 or NH_3 on the kinetic current density for the reference catalyst (Fe/KB600) and the Fe/Fe+S catalyst.

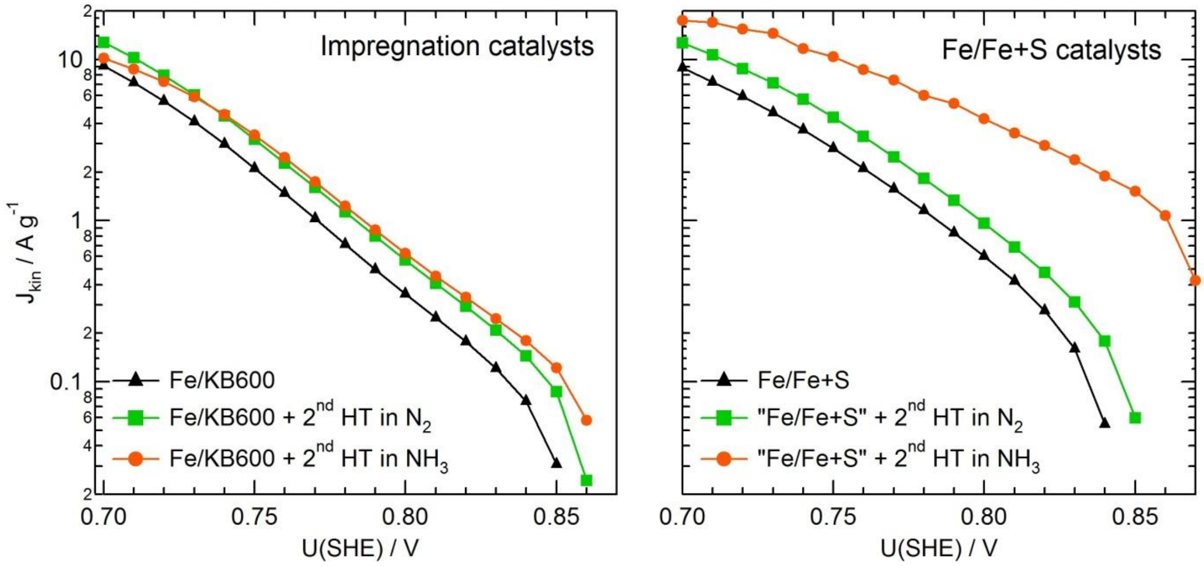

Fig. S6. Tafel plots of impregnation catalysts and Fe/Fe+S catalysts after different stages of preparation.

The reference catalyst Fe/KB600, the standard catalyst Fe/Fe+S and “Fe/Fe+S”+ 2nd HT in N_2 were prepared according to Koslowski et al..[9] The 2nd heat-treatment of Fe/KB600 in N_2 was similarly performed to “Fe/Fe +S” + 2nd HT in N_2. Both 2nd heat-treatments in ammonia were performed for 30 min at 800°C. The cooling process of these two catalysts was conducted in N_2 atmosphere.

Supplementary Information References

1 U.I. Kramm, PhD thesis, Technische Universität Berlin, 2009.

2 I. Herrmann, U.I. Kramm, S. Fiechter, and P. Bogdanoff, *Electrochim. Acta* 2009, **54**, 4275.

3 U.I. Kramm, I. Abs-Wurmbach, I. Herrmann-Geppert, J. Radnik, S. Fiechter and P. Bogdanoff, *J. Electrochem. Soc.* 2011, **158**, B69.

4 N.N. Greenwood and T.C. Gibb, *Mössbauer Spectroscopy*; 1 ed.; Chapman and Hall Ltd.: London, 1971; Vol.**1**

5 J. Blomquist, H. Lang, R. Larsson, A. Widelöv, *J. Chem. Soc., Faraday Trans.* 1992, **88**, 2007.

6 A.L. Bouwkamp-Wijnoltz, W. Visscher, J.A.R. v. Veen, E. Boellaard, A.M. v.d. Kraan, and S.C. Tang, *J. Phys. Chem. B* 2002, **106**, 12993.

7 C.A. Melendres, *J. Phys. Chem.* 1980, **84**, 1936.

8 R. Taube, *Pure & Applied Chemistry* 1974, **38**, 427.

9 U.I. Koslowski, I. Abs-Wurmbach, S. Fiechter, and P. Bogdanoff, *J. Phys. Chem. C* 2008, **112**, 15356.